mathematics

MDPI

Review

Anisotropic Flows of Charmonium in the Relativistic Heavy-Ion Collisions

Chenyu Li [1] and Baoyi Chen [2,*]

[1] Culver Academies, Academy Rd., Culver, IN 46511, USA
[2] Department of Physics, Tianjin University, Tianjin 300354, China
* Correspondence: baoyi.chen@tju.edu.cn

Abstract: We review recent studies about anisotropic flows (v_1, v_2, v_3) of charmonium in the quark-gluon plasma produced in relativistic heavy-ion collisions. Collective flows of the bulk medium are developed due to the anisotropic pressure gradient of the medium. Strongly coupled with the bulk medium, charm quarks carry collective flows from the expanding medium, which will be inherited by the regenerated charmonium via the coalescence process. In event-by-event collisions where nucleon positions fluctuate from the smooth distribution, there is triangularity in the medium initial energy density. Triangular flows of the bulk medium and heavy flavor particles can be developed due to the initial fluctuations. In the longitudinal direction, the rapidity-odd distribution of the initial energy density is induced by the rotation of the medium in non-central heavy-ion collisions. Charmonium suffers biased dissociation along positive and negative x-directions in forward (backward) rapidity. The directed flow of charmonium becomes non-zero. The directed, elliptic and triangular flows (v_1, v_2, v_3) of charmonium come from the anisotropic initial distributions of the medium energy density in the transverse and longitudinal directions.

Keywords: relativistic heavy-ion collisions; heavy quarkonium; quark-gluon plasma; collective flows

MSC: 82C10

Citation: Li, C.; Chen, B. Anisotropic Flows of Charmonium in the Relativistic Heavy-Ion Collisions. *Mathematics* **2022**, *10*, 4284. https://doi.org/10.3390/math10224284

Academic Editors: Alexandru S. Parvan and Trambak Bhattacharyya

Received: 4 October 2022
Accepted: 28 October 2022
Published: 16 November 2022

1. Introduction

In the relativistic heavy-ion collisions, an extremely hot deconfined medium consisting of quarks and gluons, also called "quark-gluon plasma" (QGP), is believed to be generated in the collision area [1]. Studying the signals and the properties of the deconfined matter, which is similar to the state of our early universe, is one of the important tasks in relativistic heavy-ion collisions. Deconfined matter is created when the energy density is above a critical value $\sim$1 GeV/fm^3 [2]. Then, the hot medium expands outside violently due to a large gradient of the energy density and turns into a hadronic medium with a first-order or crossover phase transition when the temperature drops below a critical temperature T_c [3]. The anisotropy of the energy density profile is transformed into the anisotropy of the azimuthal distribution of light hadrons [4]. Based on the theoretical and experimental studies about the anisotropic flows of light hadrons [5–8], QGP turns out to be nearly a perfect fluid with a small ratio of shear viscosity over entropy density η/s. Heavy quarks and quarkonium, which are produced at the beginning of nuclear collisions, have been suggested to be a clean probe of an early stage of the medium [9]. Compared with light hadrons, which are usually produced at the hadronization hypersurface, heavy quarkonium is more sensitive to the initial profiles of the hot medium. The color-screening effect and random scatterings with thermal partons dissociate heavy quarkonium states in the hot medium. It suppresses the nuclear modification factor R_{AA}, which is defined as the ratio of the quarkonium production in AA collisions and the production in proton-proton (pp) collisions scaled by the number of binary collisions N_{coll} [10–21]. The suppression of R_{AA} is proportional to the cold and hot nuclear matter effects, which have been observed in the

experiments at the Super Proton Synchrotron (SPS) [22], the Relativistic Heavy-Ion Collider (RHIC) [23] and the Large Hadron Collider (LHC) [24,25].

The charmonium nuclear modification factor is enhanced in AA collisions at the LHC energies, where the medium temperatures are higher than the situation at RHIC energies. The increase in charmonium R_{AA} at LHC energies is suggested to come from the coalescence of charm and anti-charm quarks in the QGP [26–32]. This coalescence contribution is proportional to the square of charm pair numbers $N_{c\bar{c}}$ in the medium and is significantly enhanced when $N_{c\bar{c}}$ becomes large. At LHC collision energies, $N_{c\bar{c}}$ is much larger than the value at RHIC and SPS energies. The p_T spectrum of regenerated charmonium depends on the distribution of charm quarks in phase space. In the expanding QGP, charm quarks are strongly coupled with the medium to dump energy and carry collective flows in the medium [33–39]. Heavy quark energy loss is determined by the coupling strength between heavy quarks and the medium. With stronger coupling strength, heavy quarks tend to reach momentum thermalization and diffuse into a larger volume with the expanding medium. Therefore, the regenerated charmonium from the kinetically thermalized charm quarks are mainly distributed at the low p_T region [40]. Charm spatial diffusions with the expanding medium reduce the probability of their coalescence into a charmonium-bound state. At the LHC energies, where the regeneration mechanism dominates charmonium production, charmonium's final distribution is closely connected with the dynamical evolutions of charm quarks in the medium.

In this manuscript, we review the recent studies about the effects of charm quark diffusions on the charmonium collective flows. To describe the dynamical evolutions of charm quarks and charmonium, the Boltzmann-type transport model [12] and the Langevin-plus-coalescence model [41] will be introduced. In the expanding medium, the diffusion of charm quarks reduces the spatial densities of charm quarks and suppresses the coalescence probability per one c and $\bar{c}$. In semi-central collisions, the elliptic flows of the medium are developed. Additional triangular flows are also observed, which is induced by the fluctuations in the distribution of initial energy density. The rotation of the hot medium also results in the rapidity-odd distribution of the medium along the longitudinal direction. Charmonium suffers from biased dissociation along the positive and negative $x-$directions in the tilted medium. The directed flow of charmonium is non-zero in forward (backward) rapidities. All of charmonium anisotropic flows in AA collisions are due to the anisotropic initial distribution of the medium energy density in the transverse and longitudinal directions, as well as the charm quark diffusions in the medium.

2. Charm Thermalization and Charmonium Regeneration

2.1. Charm Quark Evolution

As heavy quarks are stongly coupled with the quark-gluon plasma, they suffer significant energy loss and carry collective flows in the medium. Large collective flows of D-mesons have been observed in experiments where D-mesons are close to kinetic equilibrium when they move out of the medium. The dynamical evolutions of charm quarks in QGP and D-mesons in hadronic gas are regarded as Brownian motion. Heavy quarks lose energy via random scatterings with thermal partons and the gluon radiation induced by the medium. Including both hot medium effects, the time evolution of heavy quark momentum is described with the Langevin equation [42],

$$\frac{d\mathbf{p}}{dt} = -\eta\mathbf{p} + \xi + \mathbf{f_g}, \tag{1}$$

where $\mathbf{p}$ is the three-dimensional momentum of heavy quarks. The drag coefficient depends on the medium temperature T and the momentum $\eta = \kappa/(2TE)$ with the definition of the energy $E = \sqrt{m_c^2 + |\mathbf{p}|^2}$. Charm quark mass is taken as $m_c = 1.5$ GeV [41]. The dynamical evolutions of the medium local temperatures $T(\mathbf{x}, t)$ will be given by the hydrodynamic model. The momentum diffusion coefficient κ is connected with the spatial diffusion coefficient $\mathcal{D}_s$ via the relation $\kappa = 2T^2/\mathcal{D}_s$. From theoretical and experimental

studies about the elliptic flows and nuclear modification factors of D-mesons in nuclear collisions, the value of $\mathcal{D}_s(2\pi T)$ is estimated to be $5 \leq \mathcal{D}_s(2\pi T) \leq 7$ with weak dependence on temperature [43,44]. It becomes larger in the hadronic medium due to a weaker coupling strength.

In the noise term ξ, the correlation between random scatterings at different time steps have been neglected, and ξ is approximated to be a white noise satisfying the relation

$$\langle \xi^i(t)\xi^j(t')\rangle = \kappa\delta^{ij}\delta(t-t'), \tag{2}$$

where the momentum dependence has been neglected in ξ. Three directions are represented by the index, $i, j = (1, 2, 3)$. t and t' are the time points of the evolution.

In the third term, the gluon radiation induced by the medium is represented by the term $f_g = -d\mathbf{p}_g/dt$, which contributes a recoil force on heavy quarks. $\mathbf{p}_g$ is the three-dimensional momentum of an emitted gluon. Neglect the contribution from subsequent gluon emissions; in each time step Δt, the number of emitted gluons $\langle N_g\rangle$ in the time period $t \sim t + \Delta t$ is calculated with the formula [42]

$$P_{\rm rad}(t, \Delta t) = \langle N_g(t, \Delta t)\rangle = \Delta t \int dx dk_T^2 \frac{dN_g}{dx dk_T^2 dt}, \tag{3}$$

where the spectrum of emitted gluons are taken from Refs. [45,46]. When the time period Δt is small enough, the number of emitted gluons $\langle N_g\rangle$ is always smaller than the unit, and the value of $P_{\rm rad}$ can be interpreted as the probability of emitting one gluon. $x = E_g/E$ is the ratio of emitted gluons and the heavy quark energies. k_T is the transverse momentum of the emitted gluons. The radiation term dominates the energy loss of heavy quarks at high p_T region, while at low p_T regions, heavy quark energy loss is dominated by the first two terms on the right-hand side of Equation (1). In this work, we focus on the regeneration of charmonium via the coalescence of charm and anti-charm quarks, where most regenerated charmonium is located at low p_T bins.

The initial momentum distribution of heavy quarks can be calculated with the perturbative QCD model, such as the PYTHIA and FONLL model [47]. The initial spatial distribution of heavy quarks is proportional to the product of two thickness functions, $dN_{c\bar{c}}/d\mathbf{x}_T = \sigma_{pp}^{c\bar{c}} T_A(\mathbf{x}_T - \mathbf{b}/2) T_B(\mathbf{x}_T + \mathbf{b}/2)$. $\sigma_{pp}^{c\bar{c}}$ is the production cross-section of charm pairs in proton-proton collisions. $T_{A(B)} = \int dz \rho_{A(B)}(\mathbf{x}_T, z)$ is the thickness function defined as the integration of the nucleon density over the longitudinal direction. When heavy quarks move in the medium according to the Langevin equation, their positions are updated at each time step, $\mathbf{x}(t + \Delta t) = \mathbf{x}(t) + \mathbf{p}/E \cdot \Delta t$. The charm quark mass is larger than the medium temperature. The thermal production of charm pairs can be neglected, and the total number of charm pairs are conserved when they undergo Brownian motion in the medium. Heavy quarks carry the information of the initial stage of the hot medium.

2.2. Hot Medium Evolution

To explain the large collective flows of light hadrons in experiments, the QGP medium is suggested to be a nearly perfect fluid. The dynamical evolution of the medium temperatures and the velocities are well described in the hydrodynamic models. The equation of state (EoS) of the QGP and hadronic medium are taken from lattice QCD calculations and the Hadron resonance gas model, respectively [48]. In Figure 1, time evolution of the temperatures at the center of the medium are given by a MUSIC calculation [49]. The collision energy is taken as $\sqrt{s_{NN}} = 5.02$ TeV. The initial energy density profile is given by the Glauber model, where the maximum initial temperature is determined with the hadron multiplicity observed in heavy-ion collisions. The evolution of the temperature stops when it decreases to a kinetic freeze-out temperature $\sim$0.12 GeV.

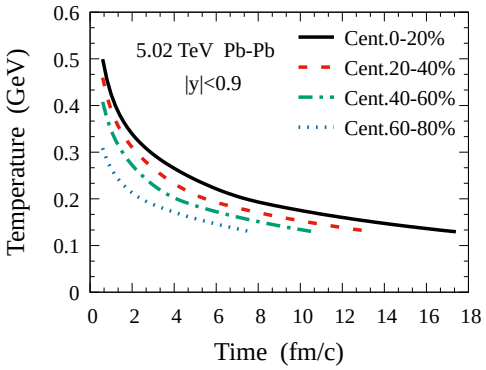

Figure 1. The time evolution of the local temperature at the center of the medium in the central rapidity in $\sqrt{s_{NN}} = 5.02$ TeV Pb-Pb collisions. The collision centrality is chosen as 0–20%, 20–40%, 40–60% and 60–80%. This temperature evolution is calculated with a MUSIC calculation. This figure is cited from Ref. [41].

3. Charmonium Thermal Production

3.1. Diffusion of Charm Quarks

With multiple charm quarks undergoing Brownian motion in the medium, uncorrelated c and $\bar{c}$, which are usually from different $c\bar{c}$ pairs, may collide with each other to form a new charmonium state. At low temperatures close to T_c, heavy quark potential is partially restored, so the newly formed charmonium state may survive from the hot medium. At LHC energies, where the number of charm pairs is large, the coalescence of c and $\bar{c}$ even dominates the final production of J/ψ and $\psi(2S)$ in Pb-Pb collisions. The coalescence probability between one random c and $\bar{c}$ quarks is written as

$$\langle \mathcal{P}_{c\bar{c}\to\psi}(\mathbf{x_M}, \mathbf{p_M})\rangle_{\text{events}} = g_M \int d\mathbf{x_1} d\mathbf{x_2} \frac{d\mathbf{p_1}}{(2\pi)^3} \frac{d\mathbf{p_2}}{(2\pi)^3} \frac{d^2N_1^{\text{norm}}}{d\mathbf{x_1} d\mathbf{p_1}} \frac{d^2N_2^{\text{norm}}}{d\mathbf{x_2} d\mathbf{p_2}} W(\mathbf{x_r}, \mathbf{q_r}) \times \delta^{(3)}(\mathbf{p_M} - \mathbf{p_1} - \mathbf{p_2}) \delta^{(3)}(\mathbf{x_M} - \frac{\mathbf{x_1} + \mathbf{x_2}}{2}), \quad (4)$$

where $\mathbf{x}_{1,2}$ and $\mathbf{p}_{1,2}$ are the positions and momentum of c and $\bar{c}$ quarks. $\frac{d^2N_1^{\text{norm}}}{d\mathbf{x_1} d\mathbf{p_1}}$ is the normalized distribution of one charm in phase space. The delta function ensures the momentum conservation in the reaction $c + \bar{c} \to \psi + g$, where the gluon momentum has been neglected for simplicity, $\mathbf{x}_M = (\mathbf{x}_1 + \mathbf{x}_2)/2$ and $\mathbf{p}_M = \mathbf{p}_1 + \mathbf{p}_2$ are the position and momentum of the formed meson. The degeneracy factor $g_M = 1/12$ is from the color and spin degrees of freedom. The Wigner function W is the Weyl transform of the charmonium wave function,

$$W(\mathbf{r}, \mathbf{q}) = \int d^3\mathbf{y} e^{-i\mathbf{q}\cdot\mathbf{y}} \psi\left(\mathbf{r} + \frac{\mathbf{y}}{2}\right) \psi^*\left(\mathbf{r} - \frac{\mathbf{y}}{2}\right), \quad (5)$$

where $\psi(\mathbf{r})$ is a charmonium wave function calculated from the Schrodinger equation with the in-medium heavy quark potential. When the wave function is approximated to be a Gaussian function, the corresponding Wigner function becomes $W(\mathbf{x_r}, \mathbf{q_r}) = 8 \exp[-\frac{{x_r}^2}{\sigma^2} - \sigma^2 {q_r}^2]$ [27]. x_r and q_r are the relative coordinates and momentum between c and $\bar{c}$ in the center of mass frame of charmonium. The information of the charmonium wave function is encoded in the Gaussian width, which is connected with the root-mean-square radius of charmonium, $\sigma^2 = \frac{4}{3} \frac{(m_1+m_2)^2}{m_1^2+m_2^2} \langle r^2 \rangle_M$ [27]. The production N_M^{AA} of charmonium in AA collisions is proportional to the square of the charm pair number $N_{c\bar{c}}^{AA}$ [41],

$$N_M^{AA} = \int d\mathbf{x_M} \frac{d\mathbf{p_M}}{(2\pi)^3} \langle \mathcal{P}_{c\bar{c}\to\psi}(\mathbf{x_M}, \mathbf{p_M}) \rangle_{\text{events}} (N_{c\bar{c}}^{AA})^2, \tag{6}$$

$$N_{c\bar{c}}^{AA} = \int d\mathbf{x_T} T_A(\mathbf{x_T} - \frac{\mathbf{b}}{2}) T_B(\mathbf{x_T} + \frac{\mathbf{b}}{2}) \mathcal{R}_S \frac{d\sigma_{pp}^{c\bar{c}}}{dy} \Delta y_{c\bar{c}}, \tag{7}$$

where the factor $\mathcal{R}_S$ represents the nuclear shadowing effect. It changes the initial distribution of charm pairs in AA collisions, especially at the LHC energies.

From Equations (4)–(6), charmonium final production depends on the dynamical evolutions of charm quarks in the medium. Strongly coupled with the medium, charm quark density is reduced by the expansion of the medium. This indicates that, in the hotter medium, it takes a longer time to cool down and restore the heavy quark potential. As a result, the charm quarks diffuse into a larger volume before they combine to form a charmonium state. This diffusion effect will suppress the coalescence probability of *one c* and *one* $\bar{c}$.

The thermal production of J/ψ at $\sqrt{s_{NN}} = 2.76$ TeV and 5.02 TeV Pb-Pb collisions are studied based on the coalescence model in Refs. [11,12,14,15,27,32]. At 5.02 TeV, J/ψ R_{AA} is enhanced due to more significant number of charm pairs in the medium compared with the situation at 2.76 TeV. However, the coalescence probability per one c and $\bar{c}$ is reduced when the time of the medium expansion is longer. This effect is characterized by the ratio $N_{J/\psi}/(N_{c\bar{c}})^2$ of J/ψ production over the square of the charm pair number, as shown in Figure 2. The ratio $N_{J/\psi}/(N_{c\bar{c}})^2$ is calculated as a function of N_p at the collision energies of $\sqrt{s_{NN}} = (2.76, 5.02, 39)$ TeV. Different time scales of charm momentum thermalization are considered in the figure. In upper and lower panels of the figure, charm quarks are assumed to reach momentum thermalization at $\tau \sim \tau_t$. Charm quarks perform free streaming before the time scale τ_t and diffuse according to the diffusion equation in $\tau > \tau_t$. In more central collisions, the initial energy density of the medium becomes larger. It takes a longer time for the medium to decrease to T_c, where the coalescence of c and $\bar{c}$ happens. The spatial density of charm quarks is diluted to reduce the coalescence probability of *one c* and $\bar{c}$. Similarly, at higher collision energies, with the production of higher energy density, the diffusion of charm quarks is more vital, and charm spatial density is more reduced.

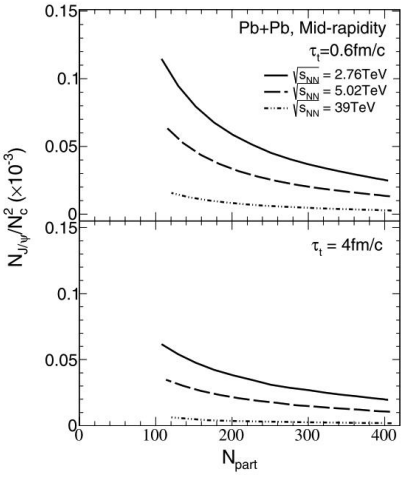

Figure 2. The ratio of J/ψ production to the square of the total charm pair number (with $N_c = N_D + N_{\Lambda_c} + \ldots$ including all charm flavor hadrons) as a function of the number of participants N_{part} in Pb-Pb collisions. The collision energies are chosen as $\sqrt{s_{NN}} = 2.76, 5.02, 39$ TeV, respectively. Charm quark momentum distribution is assumed to reach equilibrium at the beginning of medium expansion $\tau_t = 0.6$ fm/c in the upper panel and $\tau_t = 4$ fm/c in the lower panel. This figure is cited from Ref. [32].

The charm diffusion in the expanding medium tends to suppress the nuclear modification factor R_{AA}. In Figure 3, when employing the same hydrodynamic evolution at both 2.76 TeV and 5.02 TeV as a test, $R_{AA}(5.02\ TeV)$ is enhanced because of a larger production cross-section of charm pairs $d\sigma_{pp}^{c\bar{c}}/dy$ at 5.02 TeV compared with the situation at 2.76 TeV. Their ratio is plotted with blue dotted line in Figure 3. When taking the realistic evolutions for the medium produced at each collision energy, the coalescence probability per one c and $\bar{c}$ is reduced at 5.02 TeV due to a stronger diffusion of charm quarks before the coalescence process. The difference between the blue dotted line (with the same hydrodynamic evolution) and the black solid line (with two realistic hydrodynamic evolutions) are due to the different diffusions of charm quarks in two collision energies.

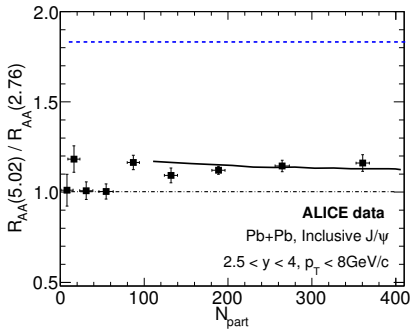

Figure 3. The ratio of inclusive nuclear modification factors R_{AA} at 2.76 TeV and 5.02 TeV Pb-Pb collisions, plotted with a black solid line. The blue dotted line is a situation where the same hydrodynamic evolution is used as a test in both collision energies. The reduction from dotted to black solid lines is due to the stronger diffusion of charm quarks in the hotter medium produced at 5.02 TeV. This figure is cited from Ref. [32].

3.2. Elliptic Flow v_2

In non-central nuclear collisions, the collision area of two nuclei is elliptic. The gradient of the initial energy density becomes anisotropic in the transverse plane. With different accelerations in the x- and y-directions, the azimuthal distribution $dN/d\phi$ of the final hadrons is anisotropic as well, which can be expanded as

$$dN/d\phi \propto 1 + 2\sum_{n=1}^{\infty} v_n \cos n(\phi - \Phi_n), \tag{8}$$

where v_n and Φ_n are the magnitude and the phase of the nth-order harmonic flows in the azimuthal angle distribution of final particles. As charm quarks are strongly coupled with the medium, charm quarks diffuse in the expanding medium to carry elliptic flows. At temperatures close to T_c where heavy quark potential is partially restored, charmonium is regenerated via the coalescence of charm quarks and inherits the collective flows of charm quarks.

In AA collisions, final charmonium comes from two mechanisms: the primordial production at the beginning of nuclear collisions and the regeneration from the coalescence of charm quarks in the QGP expansion. Charmonium bound states suffer dissociation in the hot medium. On the other hand, the regeneration process increases the final production of charmonium. Both contributions can be included in the transport equation. The charmonium distribution in phase space f_Ψ evolves with time. It can be simplified as [11,12,50,51],

$$\left[\cosh(y-\eta)\frac{\partial}{\partial\tau} + \frac{\sinh(y-\eta)}{\tau}\frac{\partial}{\partial\eta} + \mathbf{v}_T \cdot \nabla_T\right] f_\Psi = -\alpha_\Psi f_\Psi + \beta_\Psi \tag{9}$$

where τ and η are the proper time and the pseudo-rapidity, respectively. Here, y is the rapidity in momentum space. $\mathbf{v}_T = \mathbf{p}_T/E_T = \mathbf{p}_T/\sqrt{m_\Psi^2 + p_T^2}$ is the transverse velocity

of charmonium moving in the medium. The terms on the left-hand side represent the charmonium distribution f_Ψ changing with time τ and coordinates $(\eta, \mathbf{x}_T)$. On the right-hand side, α and β represent the decay rate and the regeneration rate of charmonium. The decay rate α_Ψ is proportional to the density of thermal gluons and the inelastic cross-section. The regeneration rate β_Ψ in the reaction $c + \bar{c} \to \Psi + g$ is proportional to the densities of charm and anti-charm quarks and their coalescence probability. The formulas of α_Ψ and β_Ψ are given in Equations (10) and (11),

$$\alpha_\Psi(\boldsymbol{p}, \boldsymbol{x}, \tau|\mathbf{b}) = \frac{1}{2E_T}\int \frac{d^3\boldsymbol{p}_g}{(2\pi)^3 2E_g} W^{c\bar{c}}_{g\psi}(s) f_g(\boldsymbol{p}_g, \boldsymbol{x}, \tau)\Theta(T(\boldsymbol{x}, \tau|\boldsymbol{b}) - T_c), \tag{10}$$

$$\begin{aligned}\beta_\Psi(\boldsymbol{p}, \boldsymbol{x}, \tau|\boldsymbol{b}) = {} & \frac{1}{2E_T}\int \frac{d^3\boldsymbol{p}_g}{(2\pi)^3 2E_g}\frac{d^3\boldsymbol{p}_c}{(2\pi)^3 2E_c}\frac{d^3\boldsymbol{p}_{\bar{c}}}{(2\pi)^3 2E_{\bar{c}}} \\ & \times W^{g\psi}_{c\bar{c}}(s) f_c(\boldsymbol{p}_c, \boldsymbol{x}, \tau|\boldsymbol{b}) f_{\bar{c}}(\boldsymbol{p}_{\bar{c}}, \boldsymbol{x}, \tau|\boldsymbol{b}) \\ & \times (2\pi)^4 \delta^{(4)}(p + p_g - p_c - p_{\bar{c}})\Theta(T(\boldsymbol{x}, \tau|\boldsymbol{b}) - T_c).\end{aligned} \tag{11}$$

In the above formulas, f_g is the gluon density, and $W^{c\bar{c}}_{g\psi}$ is the dissociation rate calculated from pQCD [52,53]. The step function $\Theta(T - T_c)$ ensures that the parton dissociation only exists in the QGP. In β_Ψ, $W^{g\psi}_{c\bar{c}}$ is connected with $W^{c\bar{c}}_{g\psi}$ via the detailed balance. δ functions indicate the energy-momentum conservation in the coalescence process. f_c and $f_{\bar{c}}$ are the density of c and $\bar{c}$ quarks. Their distribution can be obtained from the Langevin model. As D meson elliptic flows are large and close to the flows of light hadrons [34,54], in the thermalization limit, charm spatial density satisfies the equation $\partial_\mu(\rho_c u^\mu) = 0$, where u^μ is the four-velocity of the fluid. Charm momentum distribution is taken as a normalized Fermi distribution as an approximation.

The initial distribution of primordially produced charmonium in nuclear collisions is obtained from the production in proton-proton collisions scaled with the number of binary collisions N_{coll}. In proton-proton collisions, the p_T-spectrum of J/ψ can be parametrized with the form

$$f^{J/\psi}_{pp} \equiv \frac{d^2\sigma^{J/\psi}_{\mathrm{pp}}}{dy 2\pi p_T dp_T} = \frac{d\sigma^{J/\psi}_{\mathrm{pp}}}{dy} \times \frac{(n-1)}{\pi(n-2)\langle p_T^2\rangle_{pp}}[1 + \frac{p_T^2}{(n-2)\langle p_T^2\rangle_{pp}}]^{-n}, \tag{12}$$

where the rapidity-differential cross-section $d\sigma^{J/\psi}_{pp}/dy$ is determined by experiments [55,56]. The parameters n and $\langle p_T^2\rangle$ characterize the shape of the J/ψ p_T-distribution in pp collisions [57]. In AA collisions, the cold nuclear matter (CNM) effect also changes the production of charmonium. The nuclear shadowing effect modifies the parton densities in the nucleus, which affects the charmonium production. The partons from nucleons scatter with other nucleons before fusing into a charmonium and charm pair. This process increases the p_T of produced charmonium compared with the situation in pp collisions. It is also called the Cronin effect, which can be included by modifying $f^{J/\psi}_{pp}$ with a Gaussian smearing method. All of the cold nuclear matter effects happen before the hot medium effects. Therefore, those CNM effects are included in the initial distribution of Equation (9) [58],

$$f_\Psi(\mathbf{x}, \mathbf{p}_T, y, \tau_0) = (2\pi)^3\delta(z)T_A(\mathbf{x}_T - \mathbf{b}/2)T_B(\mathbf{x}_T + \mathbf{b}/2)\mathcal{R}^A_S\mathcal{R}^B_S\overline{f^{J/\psi}_{pp}}, \tag{13}$$

where the shadowing factor $\mathcal{R}^{A(B)}_S$ is calculated with the EPS09 NLO calculation [59]. $\overline{f^{J/\psi}_{pp}}$ is the momentum distribution of primordially produced J/ψ with the modification of Cronin effect.

Solving the transport model, the J/ψ nuclear modification factor including both primordial production and regeneration is plotted in the left panel of Figure 4. Dotted, dashed and solid lines represent the primordial production, regeneration, and inclusive production, respectively. In semi-central and central collisions, the regeneration dominates

the final production of J/ψ. The regenerated charmonium is mainly located in the low p_T region because of the charm quark energy loss. The primordial production dominates the production at high p_T. Therefore, in the right panel of Figure 4, v_2 of the final inclusive J/ψ is significant in low p_T regions because of the collective flows of charm quarks. At high p_T, v_2 is small because J/ψ as a color-singlet state is not strongly coupled with the medium, as with single charm quarks. Primordially produced charmonium performs free streaming in the medium, and the small non-zero v_2 of J/ψ is induced by the path-length difference of trajectories when they move along different directions in the transverse plane. At the high p_T region in the right panel of Figure 4, theoretical calculations underestimate the experimental data. This may be due to the non-thermal distribution of charm quarks in the medium [60].

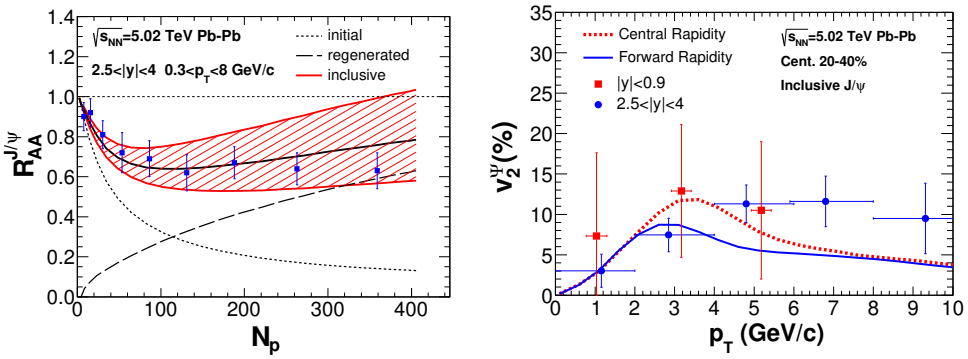

Figure 4. (**Left**) J/ψ nuclear modification factor R_{AA} as a function of number of participant N_p at $\sqrt{s_{NN}}$ = 5.02 TeV Pb-Pb collisions. Dotted, dashed and solid lines represent the primordial production, regeneration and inclusive production, respectively. The band corresponds to the uncertainty in the production cross-section of charm pair $d\sigma_{pp}^{c\bar{c}}/dy$. (**Right**) Elliptic flows of inclusive J/ψ as a function of p_T in centrality 0–20%. This figure is cited from Ref. [57].

3.3. Triangular Flow v_3

In the event-by-event heavy-ion collisions, the nucleon positions fluctuate and deviate from the smooth distribution of the nucleus [61]. The energy density produced by the collisions also fluctuate event-by-event. The realistic fluctuating profiles of the medium energy density is simulated with the Monte Carlo Glauber model (MC-Glauber) [62] and Monte Carlo fKLN model (MC-KLN) [63]. In the dynamical expansion , where the anisotropy in the initial distribution of medium energy density is transformed into the anisotropy in the momentum distribution of hadrons, there is a non-zero triangular flow in the azimuthal distribution of hadrons. In experiments, the v_3 of light hadrons have been observed and explained well with the hydrodynamic model plus the fluctuating initial conditions. The value of v_3 is proportional to the triangularity in the initial fluctuating distribution. The regenerated charmonium from the coalescence of charm quarks also carry collective flows. The magnitude of the charmonium v_3 is determined by the initial fluctuations and the degree of charm kinetic thermalization.

Firstly, one can generate a large set of fluctuating initial conditions with the Monte Carlo method. Then, we can take these fluctuating medium evolutions into the transport model to calculate the v_3 of J/ψ in each event. This calculation needs a huge computation time. Instead, one can take single-shot hydrodynamics where triangular distributions of the initial energy density from fluctuations are encoded in the initial conditions. To introduce the triangularity in the initial energy density of the medium, a deformation factor is included in the formula of the energy denstiy [64],

$$\epsilon(\boldsymbol{x}, \tau_0|\boldsymbol{b}) \to \epsilon(\tilde{\boldsymbol{x}}, \tau_0|\boldsymbol{b}), \tag{14}$$

where the deformed coordinate is $\tilde{x} = (x_T\sqrt{1+\varepsilon_3\cos[3(\phi_s-\Psi_3)]}, \phi_s, \eta)$. $x_T = \sqrt{x^2+y^2}$ and $\phi_s = \arctan(|y|/|x|)$ are the transverse radius and azimuth angle. $\Psi_3 = 0$ is regarded as the reaction plane angle in the smooth hydrodynamic evolution. The value of the parameter ϵ_3 characterizing the magnitude of the fluctuation is determined to be $\epsilon_3 = 0.08, 0.1, 0.2$ in the centrality bins 0–10%, 10–30% and 30–50%, respectively, in 5.02 TeV Pb-Pb collisions according to the simulation from the MC-Glauber or MC-KLN model [64,65]. The spatial distributions of the energy density with and without the fluctuations are plotted in Figure 5.

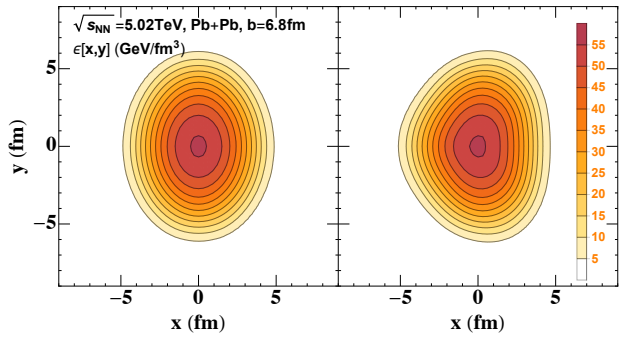

Figure 5. The initial energy density in the transverse plane in $\sqrt{s_{NN}} = 5.02$ TeV Pb-Pb collisions. In the left panel, no fluctuations are considered. In the right panel, a deformation characterizing the triangularity in the energy density is included. This figure is cited from Ref. [66].

In the left panel of Figure 5, the shape of the initial energy density is elliptic, which comes from the geometry size of the collision area. In the right panel of Figure 5, the triangular shape in the profile of the energy density is encoded, which characterizes the magnitude of the fluctuations. The corresponding elliptic and triangular flows (v_2, v_3) of J/ψ are calculated based on the transport equation by taking the corresponding hydrodynamic evolutions; please see Figure 6.

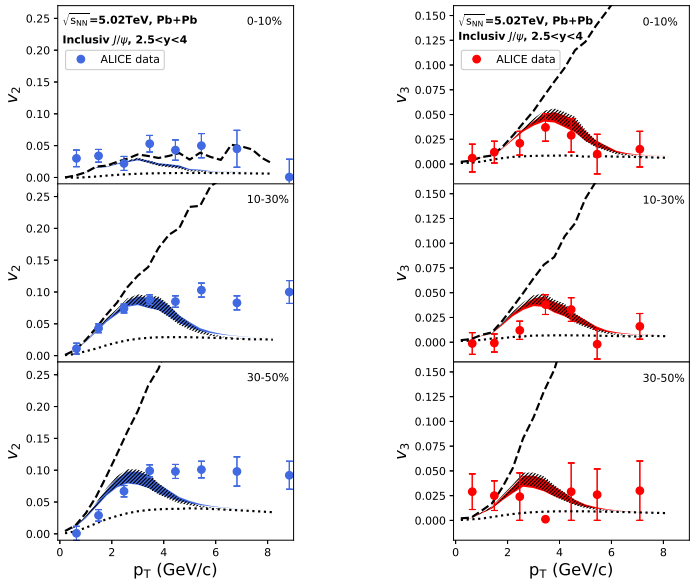

Figure 6. (**Left**) Elliptic flows of J/ψ as a function of p_T in $\sqrt{s_{NN}} = 5.02$ TeV Pb-Pb collisions. The dotted and dashed lines and shadow bands represent the elliptic flows of initially produced, regenerated and inclusive J/ψ, respectively. The collision centrality is 0–10%, 10–30%, and 30–50%, respectively. (**Right**) Triangular flows of charmonium as a function of p_T. This figure is cited from Ref. [66].

In Figure 6, elliptic flows depend sensitively on the collision centrality. In a central collision, the pressure gradient of the medium energy density is nearly isotropic in the transverse plane. Elliptic flows of the medium and heavy flavor particles are small in the centrality range of 0–10%. In a centrality range of 10–30%, the elliptic flow becomes larger due to the elliptic profile of the collision area, where medium acceleration is different along the x- and y-directions in the transverse plane. In the high p_T region, theoretical calculations underestimate the experimental data. This may be due to the non-thermal distribution of charm quarks [60]. For triangular flows, they mainly come from the fluctuation of the medium energy density, which shows relatively weak dependence on the impact parameter. The charmoniums v_3 in three centralities are close to each other without significant differences. The observation of J/ψ v_3 indicates clearly that charm quarks are strongly coupled with the medium to be affected by the fluctuations.

3.4. Directed Flow v_1

In the previous discussions, we have discussed the anisotropy of the medium initial energy density in the transverse plane. In this section, we discuss the rapidity-odd distribution of the energy density induced by the rotation of the medium in semi-central nuclear collisions. In the collision area, the nucleus moving with the positive (negative) rapidity tends to tilt the produced bulk medium to positive (negative) x with respect to the beam axis for positive (negative) z. The magnitude of the tilt in the bulk medium is connected with the directed flows of light-charged hadrons, which have been observed in experiments [67,68]. In the Au-Au collisions at RHIC energy, the rapidity distribution of the medium energy density is plotted in the centrality of 0–80%; please see the left panel of Figure 7. In the forward (backward) rapidity, the medium is tilted towards the positive (negative) x-direction. The initial entropy density of the medium is parametrized with the formula

$$s(\tau_0, \mathbf{x}_T, \eta) = s_0 \times \exp[-\theta(|\eta| - \eta_0)\frac{(|\eta| - \eta_0)^2}{2\sigma^2}] \times [c_{hard} N_{coll} + (1 - c_{hard})(N^+_{part}\zeta_+(\eta) + N^-_{part}\zeta_-(\eta))], \quad (15)$$

where s_0 and the parameters in the exponential factor characterize the initial entropy density and the rapidity-odd distribution of the medium, respectively [69]. The initial entropy density depends on both soft and hard processes, where the fractions are $(1 - c_{\text{hard}})$ and $c_{\text{hard}} = 0.05$, respectively. N^+_{part} and N^-_{part} are the number of participants in the forward and backward rapidities. The feature of the rapidity-odd distribution is introduced via the function $\zeta_{+,-}(\eta)$. The hydrodynamic evolutions of the medium in both transverse and longitudinal directions are given by the MUSIC calculation with the input of the rapidity-odd initial entropy density.

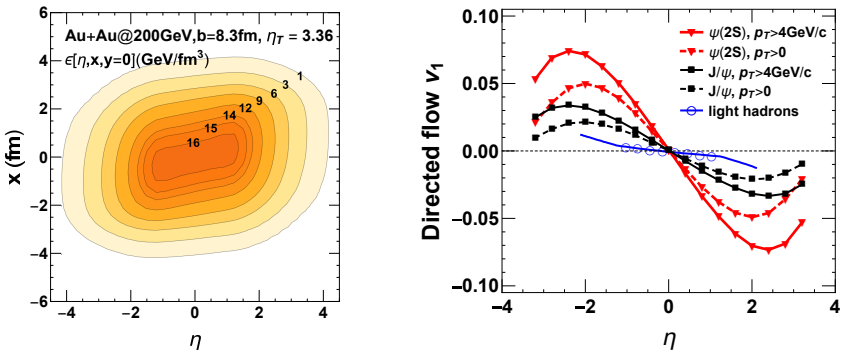

Figure 7. (**Left**) Rapidity-odd distribution of initial entropy density in $\sqrt{s_{NN}} = 200$ GeV Au-Au collisions. The collision centrality is 0–80%, corresponding to the averaged impact parameter $b = 8.3$ fm. (**Right**) The directed flows of J/ψ and $\psi(2S)$ as a function of rapidity η. Different p_T bins ($p_T > 0$ and $p_T > 4$ GeV/c) are calculated. This figure is cited from Ref. [69].

The directed flows of D mesons have been observed [70]. Compared with light hadrons, charmonium is produced in the initial parton hard scatterings where the tilted shape of the entropy distribution is apparent. Different from charm quarks, primordially produced charmonium with zero net color charge is weakly coupled with the medium. Therefore, charmonium suffers biased dissociation along the positive and negative x-directions in the tilted medium, and this information is not contaminated by the following QGP evolutions where the tilted shape of the medium is less evident. In the right panel of Figure 7, directed flows of J/ψ and $\psi(2S)$ as a function of pseudorapidity η are calculated in different p_T bins in $\sqrt{s_{NN}} = 200$ GeV Au-Au collisions [69]. As one can see, in the forward rapidity, charmonium moving along positive x-direction suffer stronger medium dissociation due to the longer path-length in the medium. This results in anisotropy in the azimuthal distribution of the final charmonium, where charmonium v_1 is negative in forward rapidity and negative in backward rapidity. For an excited state $\psi(2S)$, the binding energy is smaller than the value of the ground state. They are more easily dissociated and sensitive to the profile of the medium entropy density. In Figure 7, charmonium directed flows are bigger than the values of the light hadrons. In the above calculations regarding v_1, the regeneration process has been neglected for simplicity, which becomes less important, especially in the high p_T region where the directed flow is strong, as shown by the lines with $p_T > 4$ GeV/c in Figure 7. Confirming and quantifying the charmonium v_1 help to extract the rotation and the rapidity-odd distribution of the hot medium.

4. Summary

In the present work, we review recent studies about charmonium anisotropic flows in relativistic heavy-ion collisions. The pressure gradients of the medium energy density become different along different directions, where the acceleration of the medium expansion is also anisotropic. With strong coupling between heavy quarks and the bulk medium, charm quarks approach kinetic thermalization to carry collective flows from the expanding medium. The anisotropic flows of charm quarks will be inherited by the regenerated charmonium via the coalescence process. The elliptic flow of charmonium originates from the shape of the QGP produced in the collision area of two nuclei in semi-central collisions. It depends on the impact parameter and becomes almost zero in most central collisions. The triangular flow of charmonium comes from the fluctuations of the medium initial energy density. As the fluctuations of nucleon positions in the nucleus show weak dependence on the impact parameter, charmonium v_3 are similar to each other without evident differences in central and semi-central collisions. In the longitudinal direction, the rapidity-odd distribution of the energy density is introduced due to the rotation of the hot medium produced in non-central collisions. This results in biased charmonium dissociation along the positive and negative x-directions due to the different path-length in QGP. The directed flows of J/ψ and $\psi(2S)$ are larger than the case of light hadrons. As primordially produced charmonium is mostly dissociated by the medium in the initial stage, where the tilted shape of the medium is evident, charmonium directed flow is proposed as a sensitive probe of the profile of the medium initial energy densitiy in relativistic heavy-ion collisions.

Funding: This work is supported by the National Natural Science Foundation of China (NSFC) under Grant No. 12175165.

Data Availability Statement: Not applicable.

Conflicts of Interest: The authors declare no conflict of interest.

References

1. Bazavov, A.; Bhattacharya, T.; Cheng, M.; DeTar, C.; Ding, H.-T.; Gottlieb, S.; Gupta, R.; Hegde, P.; Heller, U.M.; Karsch, F.; et al. The chiral and deconfinement aspects of the QCD transition. *Phys. Rev. D* **2012**, *85*, 054503. [CrossRef]
2. Satz, H. Colour deconfinement and quarkonium binding. *J. Phys. G* **2006**, *32*, R25. [CrossRef]
3. Aoki, Y.; Endrődi, G.; Fodor, Z.; Katz, S.D.; Szabó, K.K. The order of the quantum chromodynamics transition predicted by the standard model of particle physics. *Nature* **2006**, *443*, 675–678. [CrossRef] [PubMed]

4. Heinz, U.; Snellings, R. Collective flow and viscosity in relativistic heavy-ion collisions. *Ann. Rev. Nucl. Part. Sci.* **2013**, *63*, 123–151. [CrossRef]
5. Song, H.; Bass, S.A.; Heinz, U.; Hirano, T.; Shen, C. 200 *A* GeV Au+Au collisions serve a nearly perfect quark-gluon liquid. *Phys. Rev. Lett.* **2011**, *106*, 192301; Erratum in *Phys. Rev. Lett.* **2012**, *109*, 139904. [CrossRef]
6. Gale, C.; Jeon, S.; Schenke, B.; Tribedy, P.; Venugopalan, R. Event-by-event anisotropic flow in heavy-ion collisions from combined Yang-Mills and viscous fluid dynamics. *Phys. Rev. Lett.* **2013**, *110*, 012302. [CrossRef]
7. Adams, J.; Aggarwal, M.M.; Ahammed, Z.; Amonett, J.; Anderson, B.D.; Arkhipkin, D.; Averichev, G.S.; Badyal, S.K.; Bai, Y.; Balewski, J.; et al. Azimuthal anisotropy in Au+Au collisions at s(NN)**(1/2) = 200-GeV. *Phys. Rev. C* **2005**, *72*, 014904. [CrossRef]
8. Aamodt, K.; Abelev, B.; Abrahantes Quintana, A.; Adamová, D.; Adare, A.M.; Aggarwal, M.M.; Aglieri Rinella, G.; Agocs, A.G.; Agostinelli, A.; Aguilar Salazar, S.; et al. Higher harmonic anisotropic flow measurements of charged particles in Pb-Pb collisions at $\sqrt{s_{NN}}$=2.76 TeV. *Phys. Rev. Lett.* **2011**, *107*, 032301. [CrossRef]
9. Matsui, T.; Satz, H. J/ψ Suppression by Quark-Gluon Plasma Formation. *Phys. Lett. B* **1986**, *178*, 416–422. [CrossRef]
10. Braun-Munzinger, P.; Stachel, J. (Non)thermal aspects of charmonium production and a new look at J/ψ suppression. *Phys. Lett. B* **2000**, *490*, 196–202. [CrossRef]
11. Zhu, X.L.; Zhuang, P.F.; Xu, N. J/ψ transport in QGP and p(t) distribution at SPS and RHIC. *Phys. Lett. B* **2005**, *607*, 107–114. [CrossRef]
12. Yan, L.; Zhuang, P.; Xu, N. Competition between J/ψ suppression and regeneration in quark-gluon plasma. *Phys. Rev. Lett.* **2006**, *97*, 232301. [CrossRef] [PubMed]
13. Liu, Y.; Chen, B.; Xu, N.; Zhuang, P. Y Production as a Probe for Early State Dynamics in High Energy Nuclear Collisions at RHIC. *Phys. Lett. B* **2011**, *697*, 32–36. [CrossRef]
14. Grandchamp, L.; Rapp, R.; Brown, G.E. In medium effects on charmonium production in heavy ion collisions. *Phys. Rev. Lett.* **2004**, *92*, 212301. [CrossRef]
15. Zhao, X.; Rapp, R. Medium Modifications and Production of Charmonia at LHC. *Nucl. Phys. A* **2011**, *859*, 114–125. [CrossRef]
16. Blaizot, J.P.; Boni, D.D.; Faccioli, P.; Garberoglio, G. Heavy quark bound states in a quark–gluon plasma: Dissociation and recombination. *Nucl. Phys. A* **2016**, *946*, 49–88. [CrossRef]
17. Krouppa, B.; Ryblewski, R.; Strickland, M. Bottomonia suppression in 2.76 TeV Pb-Pb collisions. *Phys. Rev. C* **2015**, *92*, 061901. [CrossRef]
18. Yao, X.; Ke, W.; Xu, Y.; Bass, S.A.; Müller, B. Coupled Boltzmann Transport Equations of Heavy Quarks and Quarkonia in Quark-Gluon Plasma. *J. High Energy Phys.* **2021**, *2021*, 46. [CrossRef]
19. Yao, X.; Mehen, T. Quarkonium Semiclassical Transport in Quark-Gluon Plasma: Factorization and Quantum Correction. *J. High Energy Phys.* **2021**, *2021*, 62. [CrossRef]
20. Wen, L.; Du, X.; Shi, S.; Chen, B. Probe the color screening in proton-nucleus collisions with complex potentials. *Chin. Phys. C* **2022**, *46*, 114102. [CrossRef]
21. Shi, W.; Zha, W.; Chen, B. Charmonium Coherent Photoproduction and Hadroproduction with Effects of Quark Gluon Plasma. *Phys. Lett. B* **2018**, *777*, 399–405. [CrossRef]
22. Abreu, M.C.; Alessandro, B.; Alexa, C.; Arnaldi, R.; Atayan, M.; Baglin, C.; Baldit, A.; Bedjidian, M.; Bellaiche, F.; Beolè, S.; et al. Transverse momentum distributions of J/ψ, ψ', Drell–Yan and continuum dimuons produced in Pb–Pb interactions at the SPS. *Phys. Lett. B* **2001**, *499*, 85–96. [CrossRef]
23. Adare, A.; Afanasiev, S.; Aidala, C.; Ajitanand, N.N.; Akiba, Y.; Al-Bataineh, H.; Alexander, J.; Al-Jamel, A.; Aoki, K.; Aphecetche, L.; et al. J/ψ Production versus Centrality, Transverse Momentum, and Rapidity in Au+Au Collisions at $\sqrt{s_{NN}} = 200$ GeV. *Phys. Rev. Lett.* **2007**, *98*, 232301. [CrossRef]
24. Adam, J.; Adamová, D.; Aggarwal, M.M.; Aglieri Rinella, G.; Agnello, M.; Agrawal, N.; Ahammed, Z.; Ahn, S.U.; Aimo, I.; Aiola, S.; et al. Differential studies of inclusive J/ψ and ψ(2S) production at forward rapidity in Pb-Pb collisions at $\sqrt{s_{\rm NN}} = 2.76$ TeV. *J. High Energy Phys.* **2016**, *2016*, 179. [CrossRef]
25. Adam, J.; Adamová, D.; Aggarwal, M.M.; Aglieri Rinella, G.; Agnello, M.; Agrawal, N.; Ahammed, Z.; Ahmad, S.; Ahn, S.U.; Aiola, S.; et al. J/ψ suppression at forward rapidity in Pb-Pb collisions at $\sqrt{s_{\rm NN}} = 5.02$ TeV. *Phys. Lett. B* **2017**, *766*, 212–224. [CrossRef]
26. Thews, R.L.; Schroedter, M.; Rafelski, J. Enhanced J/ψ production in deconfined quark matter. *Phys. Rev. C* **2001**, *63*, 054905. [CrossRef]
27. Greco, V.; Ko, C.M.; Rapp, R. Quark coalescence for charmed mesons in ultrarelativistic heavy ion collisions. *Phys. Lett. B* **2004**, *595*, 202–208. [CrossRef]
28. Andronic, A.; Braun-Munzinger, P.; Redlich, K.; Stachel, J. Statistical hadronization of charm in heavy ion collisions at SPS, RHIC and LHC. *Phys. Lett. B* **2003**, *571*, 36–44. [CrossRef]
29. Fries, R.J.; Greco, V.; Sorensen, P. Coalescence Models For Hadron Formation From Quark Gluon Plasma. *Ann. Rev. Nucl. Part. Sci.* **2008**, *58*, 177–205. [CrossRef]
30. Du, X.; Rapp, R. Sequential Regeneration of Charmonia in Heavy-Ion Collisions. *Nucl. Phys. A* **2015**, *943*, 147–158. [CrossRef]
31. Chen, B.; Zhao, J. Bottomonium Continuous Production from Unequilibrium Bottom Quarks in Ultrarelativistic Heavy Ion Collisions. *Phys. Lett. B* **2017**, *772*, 819–824. [CrossRef]

32. Zhao, J.; Chen, B. Strong diffusion effect of charm quarks on J $/\psi$ production in Pb–Pb collisions at the LHC. *Phys. Lett. B* **2018**, *776*, 17–21. [CrossRef]
33. Chatrchyan, S.; Khachatryan, V.; Sirunyan, A.M.; Tumasyan, A.; Adam, W.; Bergauer, T.; Dragicevic, M.; Erö, J.; Fabjan, C.; Friedl, M.; et al. Suppression of non-prompt J/ψ, prompt J/ψ, and Y(1S) in PbPb collisions at $\sqrt{s_{NN}} = 2.76$ TeV. *J. High Energy Phys.* **2012**, *2012*, 63.
34. Abelev, B.; Adam, J.; Adamová, D.; Adare, A.M.; Aggarwal, M.M.; Rinella, G.A.; Agnello, M.; Agocs, A.G.; Agostinelli, A.; Ahammed, Z.; et al. D meson elliptic flow in non-central Pb-Pb collisions at $\sqrt{s_{\rm NN}}$ = 2.76TeV. *Phys. Rev. Lett.* **2013**, *111*, 102301. [CrossRef] [PubMed]
35. Cao, S.; Qin, G.Y.; Bass, S.A. Heavy-quark dynamics and hadronization in ultrarelativistic heavy-ion collisions: Collisional versus radiative energy loss. *Phys. Rev. C* **2013**, *88*, 044907. [CrossRef]
36. Cao, S.; Coci, G.; Das, S.K.; Ke, W.; Liu, S.Y.F.; Plumari, S.; Song, T.; Xu, Y.; Aichelin, J.; Bass, S.; et al. Toward the determination of heavy-quark transport coefficients in quark-gluon plasma. *Phys. Rev. C* **2019**, *99*, 054907. [CrossRef]
37. He, M.; Fries, R.J.; Rapp, R. $\mathbf{D_s}$-Meson as Quantitative Probe of Diffusion and Hadronization in Nuclear Collisions. *Phys. Rev. Lett.* **2013**, *110*, 112301. [CrossRef]
38. He, M.; Rapp, R. Hadronization and Charm-Hadron Ratios in Heavy-Ion Collisions. *Phys. Rev. Lett.* **2020**, *124*, 042301. [CrossRef]
39. Chen, B. Elliptic flow as a probe for $\psi(2S)$ production mechanism in relativistic heavy ion collisions. *Phys. Rev. C* **2017**, *95*, 034908. [CrossRef]
40. Liu, Y.P.; Qu, Z.; Xu, N.; Zhuang, P.F. J/ψ Transverse Momentum Distribution in High Energy Nuclear Collisions at RHIC. *Phys. Lett. B* **2009**, *678*, 72–76. [CrossRef]
41. Chen, B.; Jiang, L.; Liu, X.H.; Liu, Y.; Zhao, J. $X(3872)$ Production in Relativistic Heavy-Ion Collisions. *Phys. Rev. C* **2022**, *105*, 054901. [CrossRef]
42. Cao, S.; Qin, G.Y.; Bass, S.A. Energy loss, hadronization and hadronic interactions of heavy flavors in relativistic heavy-ion collisions. *Phys. Rev. C* **2015**, *92*, 024907. [CrossRef]
43. Rapp, R.; Gossiaux, P.B.; Andronic, A.; Averbeck, R.; Masciocchi, S.; Beraudo, A.; Bratkovskaya, E.; Braun-Munzinger, P.; Cao, S.; Dainese, A.; et al. Extraction of Heavy-Flavor Transport Coefficients in QCD Matter. *Nucl. Phys. A* **2018**, *979*, 21–86. [CrossRef]
44. Zhao, J.; Zhou, K.; Chen, S.; Zhuang, P. Heavy flavors under extreme conditions in high energy nuclear collisions. *Prog. Part. Nucl. Phys.* **2020**, *114*, 103801. [CrossRef]
45. Guo, X.f.; Wang, X.N. Multiple scattering, parton energy loss and modified fragmentation functions in deeply inelastic e A scattering. *Phys. Rev. Lett.* **2000**, *85*, 3591–3594. [CrossRef]
46. Zhang, B.W.; Wang, E.; Wang, X.N. Heavy quark energy loss in nuclear medium. *Phys. Rev. Lett.* **2004**, *93*, 072301. [CrossRef]
47. Cacciari, M.; Frixione, S.; Nason, P. The p(T) spectrum in heavy flavor photoproduction. *J. High Energy Phys.* **2001**, *2001*, 6. [CrossRef]
48. Huovinen, P.; Petreczky, P. QCD Equation of State and Hadron Resonance Gas. *Nucl. Phys. A* **2010**, *837*, 26–53. [CrossRef]
49. Schenke, B.; Jeon, S.; Gale, C. (3+1)D hydrodynamic simulation of relativistic heavy-ion collisions. *Phys. Rev. C* **2010**, *82*, 014903. [CrossRef]
50. Chen, B. Detailed rapidity dependence of J/ψ production at energies available at the Large Hadron Collider. *Phys. Rev. C* **2016**, *93*, 054905. [CrossRef]
51. Chen, B.; Liu, Y.; Zhou, K.; Zhuang, P. ψ' Production and B Decay in Heavy Ion Collisions at LHC. *Phys. Lett. B* **2013**, *726*, 725–728. [CrossRef]
52. Peskin, M.E. Short Distance Analysis for Heavy Quark Systems. 1. Diagrammatics. *Nucl. Phys. B* **1979**, *156*, 365–390. [CrossRef]
53. Bhanot, G.; Peskin, M.E. Short Distance Analysis for Heavy Quark Systems. 2. Applications. *Nucl. Phys. B* **1979**, *156*, 391–416. [CrossRef]
54. Abelev, B.; Adam, J.; Adamová, D.; Adare, A.M.; Aggarwal, M.M.; Rinella, G.A.; Agocs, A.G.; Agostinelli, A.; Salazar, S.A.; Ahammed, Z.; et al. [ALICE], Anisotropic flow of charged hadrons, pions and (anti-)protons measured at high transverse momentum in Pb-Pb collisions at $\sqrt{s_{NN}}$=2.76 TeV. *Phys. Lett. B* **2013**, *719*, 18–28. [CrossRef]
55. Abelev, B.; Adam, J.; Adamová, D.; Adare, A.M.; Aggarwal, M.M.; Rinella, G.A.; Agocs, A.G.; Agostinelli, A.; Salazar, S.A.; Ahammed, Z.; et al. [ALICE], Inclusive J/ψ production in pp collisions at $\sqrt{s} = 2.76$ TeV. *Phys. Lett. B* **2012**, *718*, 295–306; Erratum in *Phys. Lett. B* **2015**, *748*, 472–473. [CrossRef]
56. Abelev, B.; Adam, J.; Adamova, D.; Adare, A.M.; Aggarwal, M.; Rinella, G.A.; Agocs, A.G.; Agostinelli, A.; Salazar, S.A.; Ahammed, Z.; et al. Measurement of prompt J/ψ and beauty hadron production cross sections at mid-rapidity in pp collisions at $\sqrt{s} = 7$ TeV. *J. High Energy Phys.* **2012**, *2012*, 65.
57. Chen, B. Thermal production of charmonia in Pb-Pb collisions at $\sqrt{s_{NN}} = 5.02$ TeV. *Chin. Phys. C* **2019**, *43*, 124101. [CrossRef]
58. Chen, B.; Guo, T.; Liu, Y.; Zhuang, P. Cold and Hot Nuclear Matter Effects on Charmonium Production in p+Pb Collisions at LHC Energy. *Phys. Lett. B* **2017**, *765*, 323–327. [CrossRef]
59. Eskola, K.J.; Paukkunen, H.; Salgado, C.A. EPS09—A New Generation of NLO and LO Nuclear Parton Distribution Functions. *J. High Energy Phys.* **2009**, *2009*, 65. [CrossRef]
60. He, M.; Wu, B.; Rapp, R. Collectivity of J/ψ Mesons in Heavy-Ion Collisions. *Phys. Rev. Lett.* **2022**, *128*, 162301. [CrossRef]
61. Alver, B.; Roland, G. Collision geometry fluctuations and triangular flow in heavy-ion collisions. *Phys. Rev. C* **2010**, *81*, 054905; Erratum in *Phys. Rev. C* **2010**, *82*, 039903. [CrossRef]

62. Miller, M.L.; Reygers, K.; Sanders, S.J.; Steinberg, P. Glauber modeling in high energy nuclear collisions. *Ann. Rev. Nucl. Part. Sci.* **2007**, *57*, 205–243. [CrossRef]
63. Kharzeev, D.; Levin, E. Manifestations of high density QCD in the first RHIC data. *Phys. Lett. B* **2001**, *523*, 79–87. [CrossRef]
64. Alver, B.H.; Gombeaud, C.; Luzum, M.; Ollitrault, J.Y. Triangular flow in hydrodynamics and transport theory. *Phys. Rev. C* **2010**, *82*, 034913. [CrossRef]
65. Qiu, Z.; Heinz, U.W. Event-by-event shape and flow fluctuations of relativistic heavy-ion collision fireballs. *Phys. Rev. C* **2011**, *84*, 024911. [CrossRef]
66. Zhao, J.; Chen, B.; Zhuang, P. Charmonium triangular flow in high energy nuclear collisions. *Phys. Rev. C* **2022**, *105*, 034902. [CrossRef]
67. Abelev, B.I.; Aggarwal, M.M.; Ahammed, Z.; Anderson, B.D.; Arkhipkin, D.; Averichev, G.S.; Bai, Y.; Balewski, J.; Barannikova, O.; Barnby, L.S.; et al. System-size independence of directed flow at the Relativistic Heavy-Ion Collider. *Phys. Rev. Lett.* **2008**, *101*, 252301. [CrossRef]
68. Adamczyk, L.; Adkins, J.K.; Agakishiev, G.; Aggarwal, M.M.; Ahammed, Z.; Alekseev, I.; Alford, J.; Anson, C.D.; Aparin, A.; Arkhipkin, D.; et al. Beam-Energy Dependence of the Directed Flow of Protons, Antiprotons, and Pions in Au+Au Collisions. *Phys. Rev. Lett.* **2014**, *112*, 162301. [CrossRef]
69. Chen, B.; Hu, M.; Zhang, H.; Zhao, J. Probe the tilted Quark-Gluon Plasma with charmonium directed flow. *Phys. Lett. B* **2020**, *802*, 135271. [CrossRef]
70. Adam, J.; Adamczyk, L.; Adams, J.R.; Adkins, J.K.; Agakishiev, G.; Aggarwal, M.M.; Ahammed, Z.; Alekseev, I.; Anderson, D.M.; Aoyama, R.; et al. First Observation of the Directed Flow of D^0 and $\overline{D^0}$ in Au+Au Collisions at $\sqrt{s_{\mathrm{NN}}}$ = 200 GeV. *Phys. Rev. Lett.* **2019**, *123*, 162301. [CrossRef]